Stochastic Gradient Geodesic MCMC Methods

Chang Liu[†], **Jun Zhu**[†], **Yang Song**[‡*]
[†] Dept. of Comp. Sci. & Tech., TNList Lab; Center for Bio-Inspired Computing Research
[†] State Key Lab for Intell. Tech. & Systems, Tsinghua University, Beijing, China
[‡] Dept. of Physics, Tsinghua University, Beijing, China
{chang-li14@mails, dcszj@}.tsinghua.edu.cn; songyang@stanford.edu

Abstract

We propose two stochastic gradient MCMC methods for sampling from Bayesian posterior distributions defined on Riemann manifolds with a known geodesic flow, e.g. hyperspheres. Our methods are the first scalable sampling methods on these manifolds, with the aid of stochastic gradients. Novel dynamics are conceived and 2nd-order integrators are developed. By adopting embedding techniques and the geodesic integrator, the methods do not require a global coordinate system of the manifold and do not involve inner iterations. Synthetic experiments show the validity of the method, and its application to the challenging inference for spherical topic models indicate practical usability and efficiency.

1 Introduction

Dynamics-based Markov Chain Monte Carlo methods (D-MCMCs) are sampling methods using dynamics simulation for state transition in a Markov chain. They have become a workhorse for Bayesian inference, with well-known examples like Hamiltonian Monte Carlo (HMC) [21] and stochastic gradient Langevin dynamics (SGLD) [28]. Here we consider variants for sampling from distributions defined on Riemann manifolds. Overall, geodesic Monte Carlo (GMC) [7] stands out for its notable performance on manifolds with known geodesic flow, such as simplex, hypersphere and Stiefel manifold [25, 16]. Its applicability to manifolds with no global coordinate systems (e.g. hyperspheres) is enabled by the embedding technique, and its geodesic integrator eliminates inner (within one step in dynamics simulation) iteration to ensure efficiency. It is also used for efficient sampling from constraint distributions [17]. Constrained HMC (CHMC) [6] aims at manifolds defined by a constraint in some $\mathbb{R}^n$. It covers all common manifolds, but inner iteration makes it less appealing. Other D-MCMCs involving Riemann manifold, e.g. Riemann manifold Langevin dynamics (RMLD) and Riemann manifold HMC (RMHMC) [13], are invented for better performance but still on the task of sampling in Euclidean space, where the target variable is treated as the global coordinates of some distribution manifold. Although they can be used to sample in non-Euclidean Riemann manifolds by replacing the distribution manifold with the target manifold, a global coordinate system of the target manifold is required. Moreover, RMHMC suffers from expensive inner iteration.

However, GMC scales undesirably to large datasets, which are becoming common. An effective strategy to scale up D-MCMCs is by randomly sampling a subset to estimate a noisy but unbiased stochastic gradient, with stochastic gradient MCMC methods (SG-MCMCs). Welling et al. [28] pioneered in this direction by developing stochastic gradient Langevin dynamics (SGLD). Chen et al. [9] apply the idea to HMC with stochastic gradient HMC (SGHMC), where a non-trivial dynamics with friction has to be conceived. Ding et at. [10] propose stochastic gradient Nosé-Hoover thermostats (SGNHT) to automatically adapt the friction to the noise by a thermostats. To unify dynamics used for SG-MCMCs, Ma et al. [19] develop a complete recipe to formulate the dynamics.

*JZ is the corresponding author; YS is with Department of Computer Science, Stanford University, CA.

29th Conference on Neural Information Processing Systems (NIPS 2016), Barcelona, Spain.

Table 1: A summary of some D-MCMCs. –: sampling on manifold not supported; †: The integrators are not in the SSI scheme (It is unclear whether the claimed "2nd-order" is equivalent to ours); ‡: 2nd-order integrators for SGHMC and mSGNHT are developed by [8] and [18], respectively.

methods	stochastic gradient	no inner iteration	no global coordinates	order of integrator
GMC [7]	×	√	√	2nd
RMLD [13]	×	√	×	1st
RMHMC [13]	×	×	×	2nd†
CHMC [6]	×	×	√	2nd†
SGLD [28]	√	√	–	1st
SGHMC [9] / SGNHT [10]	√	√	–	1st‡
SGRLD [22] / SGRHMC [19]	√	√	×	1st
SGGMC / gSGNHT (proposed)	√	√	√	2nd

In this paper, we present two SG-MCMCs for manifolds with known geodesic flow: stochastic gradient geodesic Monte Carlo (SGGMC) and geodesic stochastic gradient Nosé-Hoover thermostats (gSGNHT). They are the first scalable sampling methods on manifolds with known geodesic flow and no global coordinate systems. We use the recipe [19] to tackle the non-trivial dynamics conceiving task. Our novel dynamics are also suitable for developing 2nd-order integrators by adopting the *symmetric splitting integrator* (SSI) [8] scheme. A key property of a Kth-order integrator is the bias of the expected sample average at iteration L can be upper bounded by $L^{-K/(K+1)}$ and the mean square error by $L^{-2K/(2K+1)}$ [8], so a higher order integrator basically performs better. Our integrators also incorporate the geodesic integrator to avoid inner iteration. Our methods can also be used to scalably sample from constraint distributions [17] like GMC.

There exist other SG-MCMCs on Riemann manifold, e.g. SGRLD [22] and SGRHMC [19], stochastic gradient versions of RMLD and RMHMC respectively. But they also require the Riemann manifold to have a global coordinate system, like their original versions as is mentioned above. So basically they cannot draw samples from hyperspheres, while our methods are capable. Technically, SGRLD/SGRHMC (and RMLD/RMHMC) samples in the coordinate space, so we need a global one to make it valid. The explicit use of the Riemann metric tensor also makes the methods more difficult to implement. Our methods (and GMC) sample in the isometrically embedded space, where the whole manifold is represented and the Riemann metric tensor is implicitly embodied by the isometric embedding. Moreover, our integrators are of a higher order. Tab. 1 summarizes the key properties of aforementioned D-MCMCs, where our advantages are clearly shown.

Finally, we apply our samplers to perform inference for spherical admixture models (SAM) [23]. SAM defines a hierarchical generative process to describe the data that are expressed as unit vectors (i.e., elements on the hypersphere). The task of posterior inference is to identify a set of latent topics, which are also unit vectors. This process is highly challenging due to a non-conjugate structure and the strict manifold constraints. None of the existing MCMC methods is both applicable to the task and scalable. We demonstrate that our methods are the most efficient methods to learn SAM on large datasets, with a good performance on testing data perplexity.

2 Preliminaries

We briefly review the basics of SG-MCMCs. Consider a Bayesian model with latent variable q, prior $\pi_0(q)$ and likelihood $\pi(x|q)$. Given a dataset $\mathcal{D} = \{x_d\}_{d=1}^D$, sampling from the posterior $\pi(q|\mathcal{D})$ by D-MCMCs requires computing the gradient of potential energy $\nabla U(q) \triangleq -\nabla \log \pi(q|\mathcal{D}) = -\nabla \log \pi_0(q) - \sum_{d=1}^D \nabla \log \pi(x_d|q)$, which is linear to data size D thus not scalable. SG-MCMCs address this challenge by randomly drawing a subset $\mathcal{S}$ of $\mathcal{D}$ to build the stochastic gradient $\nabla_q \tilde{U}(q) \triangleq -\nabla_q \log \pi_0(q) - \frac{D}{|\mathcal{S}|} \sum_{x \in \mathcal{S}} \nabla_q \log \pi(x|q)$, a noisy but unbiased estimate.Under the i.i.d. assumption of $\mathcal{D}$, the central limit theorem holds: in the sense of convergence in distribution for large D,

$$\nabla_q \tilde{U}(q) = \nabla_q U(q) + \mathcal{N}(0, V(q)), \tag{1}$$

where we use $\mathcal{N}(\cdot, \cdot)$ to denote a Gaussian random variable and $V(q)$ is some covariance matrix.

The gradient noise raises challenging restrictions to the SG-MCMC dynamics. Ma et al. [19] then provide a recipe to construct correct dynamics. It claims that for a random variable z, given a Hamiltonian $H(z)$, a skew-symmetric matrix (curl matrix) $Q(z)$ and a positive definite matrix (diffusion matrix) $D(z)$, the dynamics defined by the following stochastic differential equation (SDE)

$$\mathrm{d}z = f(z)\mathrm{d}t + \sqrt{2D(z)}\mathrm{d}W(t) \tag{2}$$

has the unique stationary distribution $\pi(z) \propto \exp\{-H(z)\}$, where $W(t)$ is the Wiener process and

$$f(z) = -\left[D(z) + Q(z)\right]\nabla_z H(z) + \Gamma(z), \quad \Gamma_i(z) = \sum_j \frac{\partial}{\partial z_j}\left(D_{ij}(z) + Q_{ij}(z)\right). \tag{3}$$

The above dynamics is compatible with stochastic gradient. For SG-MCMCs, z is usually an augmentation of the target variable q, and the Hamiltonian usually follows the form $H(z) = T(z) + U(q)$. Referring to Eqn. (1), $\nabla_q \tilde{H}(z) = \nabla_q H(z) + \mathcal{N}(0, V(q))$ and $\tilde{f}(z) = f(z) + \mathcal{N}(0, B(z))$, where $B(z)$ is the covariance matrix of the Gaussian noise passed from $\nabla_z \tilde{H}(z)$ to $\tilde{f}(z)$ through Eqn. (3). We informally rewrite $\mathrm{d}W(t)$ as $\mathcal{N}(0, \mathrm{d}t)$ and express dynamics Eqn. (2) as

$$\begin{aligned}\mathrm{d}z =& f(z)\mathrm{d}t + \mathcal{N}(0, 2D(z)\mathrm{d}t) = f(z)\mathrm{d}t + \mathcal{N}(0, B(z)\mathrm{d}t^2) + \mathcal{N}\big(0, 2D(z)\mathrm{d}t - B(z)\mathrm{d}t^2\big) \\ =& \tilde{f}(z)\mathrm{d}t + \mathcal{N}\big(0, 2D(z)\mathrm{d}t - B(z)\mathrm{d}t^2\big).\end{aligned} \tag{4}$$

This tells us that the same dynamics can be exactly expressed by stochastic gradient. Moreover, the recipe is complete: for any continuous Markov process defined by Eqn. (2) with a unique stationary distribution $\pi(z) \propto \exp\{-H(z)\}$, there exists a skew-symmetric matrix $Q(z)$ so that Eqn. (3) holds.

3 Stochastic Gradient Geodesic MCMC Methods

We now formally develop our SGGMC and gSGNHT. We will describe the task settings, develop the dynamics, and show how to simulate by the 2nd-order integrators and stochastic gradient.

3.1 Technical Descriptions of the Settings

We first describe a Riemann manifold. Main concepts are depicted in Fig. 1. Let $\mathcal{M}$ be an m-dim Riemann manifold, which is covered by a set of local coordinate systems. Denote one of them by $(\mathcal{N}, \Phi)$, where $\mathcal{N} \subseteq \mathcal{M}$ is an open subset, and $\Phi : \mathcal{N} \to \Omega, Q \mapsto q$ with $\Omega \triangleq \Phi(\mathcal{N}) \subseteq \mathbb{R}^m$, $Q \in \mathcal{N}$ and $q \in \Omega$ is a homeomorphism. Additionally, transition mappings between any two intersecting local coordinate systems are required to be smooth. Denote the Riemann metric tensor under $(\mathcal{N}, \Phi)$ by $G(q)$, an $m \times m$ symmetric positive-definite matrix.

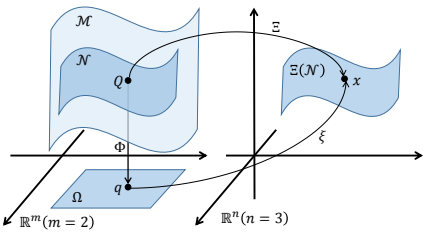

Figure 1: An illustration of manifold $\mathcal{M}$ with local coordinate system $(\mathcal{N}, \Phi)$ and embedding Ξ. See text for details.

Another way to describe $\mathcal{M}$ is through *embedding* — a smooth injection $\Xi : \mathcal{M} \to \mathbb{R}^n$ $(n \geq m)$. In $(\mathcal{N}, \Phi)$, Ξ can be embodied by a more sensible mapping $\xi \triangleq \Xi \circ \Phi^{-1} : \mathbb{R}^m \to \mathbb{R}^n, q \mapsto x$, which links the coordinate space and the embedded space. For convenience, we only consider *isometric* embeddings: Ξ such that $G(q)_{ij} = \sum_{l=1}^n \frac{\partial \xi_l(q)}{\partial q_i}\frac{\partial \xi_l(q)}{\partial q_j}, 1 \leq i, j \leq m$ holds for any local coordinate system. Common manifolds are subsets of some $\mathbb{R}^n$, in which case the identity mapping (as Ξ) from $\mathbb{R}^n$ (where $\mathcal{M}$ is defined) to $\mathbb{R}^n$ (the embedded space) is isometric.

To define a distribution on a Riemann manifold, from which we want to sample, we need a measure. In the coordinate space $\mathbb{R}^m$, Ω naturally possesses the Lebesgue measure $\lambda^m(\mathrm{d}q)$, and the probability density can be defined in Ω, which we denote as $\pi(q)$. In the embedded space $\mathbb{R}^n$, $\Xi(\mathcal{N})$ naturally possesses the Hausdorff measure $\mathcal{H}^m(\mathrm{d}x)$, and we denote the probability density w.r.t this measure as $\pi_{\mathcal{H}}(x)$. The relation between them can be found by $\pi_{\mathcal{H}}(\xi(q)) = \pi(q)/\sqrt{|G(q)|}$.

3.2 The Dynamics

We now construct our dynamics using the recipe [19] so that our dynamics naturally have the desired stationary distribution, leading to correct samples. It is important to note that the recipe only suits for dynamics in a Euclidean space. So we can only develop the dynamics in the coordinate space but not in the embedded space $\Xi(\mathcal{M})$, which is generally not Euclidean. However it is advantageous to simulate the dynamics in the embedded space (See Sec. 3.3).

Dynamics for SGGMC Define the momentum in the coordinate space $p \in \mathbb{R}^m$ and the augmented variable $z = (q, p) \in \mathbb{R}^{2m}$. Define the Hamiltonian [2] $H(z) = U(q) + \frac{1}{2}\log|G(q)| + \frac{1}{2}p^\top G(q)^{-1}p$,

[2] Another derivation of the momentum and the Hamiltonian originated from physics in both coordinate and embedded spaces is provided in Appendix C.

where $U(q) \triangleq -\log \pi(q)$. We define the Hamiltonian so that the canonical distribution $\pi(z) \propto \exp\{-H(z)\}$ marginalized w.r.t p recovers the target distribution $\pi(q)$. For a symmetric positive definite $n \times n$ matrix C, define the diffusion matrix $D(z)$ and the curl matrix $Q(z)$ as

$$D(z) = \begin{pmatrix} 0 & 0 \\ 0 & M(q)^\top C M(q) \end{pmatrix}, \; Q(z) = \begin{pmatrix} 0 & -I \\ I & 0 \end{pmatrix},$$

where we define $M(q)_{n\times m} : M(q)_{ij} = \partial \xi_i(q)/\partial q_j$. So from Eqn. (2, 3), the dynamics

$$\begin{cases} \mathrm{d}q = G^{-1} p \mathrm{d}t \\ \mathrm{d}p = -\nabla_q U \mathrm{d}t - \frac{1}{2}\nabla_q \log|G| \mathrm{d}t - M^\top C M G^{-1} p \, \mathrm{d}t - \frac{1}{2}\nabla_q \big[p^\top G^{-1} p\big] \mathrm{d}t + \mathcal{N}(0, 2M^\top C M \mathrm{d}t) \end{cases} \tag{5}$$

has a unique stationary distribution $\pi(z) \propto \exp\{-H(z)\}$.

Dynamics for gSGNHT Define $z = (q, p, \xi) \in \mathbb{R}^{2m+1}$, where $\xi \in \mathbb{R}$ is the thermostats. For a positive $C \in \mathbb{R}$, define the Hamiltonian $H(z) = U(q) + \frac{1}{2}\log|G(q)| + \frac{1}{2}p^\top G(q)^{-1} p + \frac{m}{2}(\xi - C)^2$, whose marginalized canonical distribution is $\pi(q)$ as desired. Define $D(z)$ and $Q(z)$ as

$$D(z) = \begin{pmatrix} 0 & 0 & 0 \\ 0 & CG(q) & 0 \\ 0 & 0 & 0 \end{pmatrix}, \; Q(z) = \begin{pmatrix} 0 & -I & 0 \\ I & 0 & p/m \\ 0 & -p^\top/m & 0 \end{pmatrix},$$

Then by Eqn. (2, 3) the proper dynamics of gSGNHT is

$$\begin{cases} \mathrm{d}q = G^{-1} p \mathrm{d}t \\ \mathrm{d}p = -\nabla_q U \mathrm{d}t - \frac{1}{2}\nabla_q \log|G| \mathrm{d}t - \xi p \, \mathrm{d}t - \frac{1}{2}\nabla_q \big[p^\top G^{-1} p\big] \mathrm{d}t + \mathcal{N}(0, 2CG \mathrm{d}t) \\ \mathrm{d}\xi = (\frac{1}{m} p^\top G^{-1} p - 1)\mathrm{d}t \end{cases}. \tag{6}$$

These two dynamics are novel. They are extensions of the dynamics of SGHMC and SGNHT to Riemann manifolds, respectively. Conceiving the dynamics in this form is also intended for the convenience to develop 2nd-order geodesic integrators, which differs from SGRHMC.

3.3 Simulation with 2nd-order Geodesic Integrators

In this part we develop our integrators by following the *symmetric splitting integrator* (SSI) scheme [8], which is guaranteed to be of 2nd-order. The idea of SSI is to first split the dynamics into parts with each analytically solvable, then alternately simulate each exactly with the analytic solutions. Although also SSI, the integrator of GMC does not fit our dynamics where diffusion arises. But we adopt its embedding technique to get rid of any local coordinate system thus release the global coordinate system requirement. So we will solve and simulate the split dynamics in the isometrically embedded space, where everything is expressed by the position $x = \xi(q)$ and the velocity $v = \dot{x}$ (which is actually the momentum in the isometrically embedded space, see Appendix C; the overhead dot means time derivative), instead of q and p.

Integrator for SGGMC We first split dynamics (5) into sub-SDEs with each analytically solvable:

$$A: \begin{cases} \mathrm{d}q = G^{-1} p \mathrm{d}t \\ \mathrm{d}p = -\frac{1}{2}\nabla_q \big[p^\top G^{-1} p\big] \mathrm{d}t \end{cases}, B: \begin{cases} \mathrm{d}q = 0 \\ \mathrm{d}p = -M^\top C M G^{-1} p \mathrm{d}t \end{cases}, O: \begin{cases} \mathrm{d}q = 0 \\ \mathrm{d}p = -\nabla_q U(q)\mathrm{d}t - \frac{1}{2}\nabla_q \log|G(q)|\mathrm{d}t \\ \qquad + \mathcal{N}(0, 2M^\top C M \mathrm{d}t) \end{cases}.$$

As noted in GMC, the solution of dynamics A is the geodesic flow of the manifold [1]. Intuitively, dynamics A describes motion with no force so a particle moves freely on the manifold, e.g. the *uniform motion* in Euclidean space, and motion along *great circles* (velocity rotating with varying tangents along the trajectory) on hypersphere $\mathbb{S}^{d-1} \triangleq \{x \in \mathbb{R}^d | \|x\| = 1\}$ ($\|\cdot\|$ denotes ℓ_2-norm). The evolution of the position and velocity of this kind is the geodesic flow. We require an explicit form of the geodesic flow in the embedded space. For $\mathbb{S}^{d-1}$,

$$\begin{cases} x(t) = x(0)\cos(\alpha t) + \big(v(0)/\alpha\big)\sin(\alpha t) \\ v(t) = -\alpha x(0)\sin(\alpha t) + v(0)\cos(\alpha t) \end{cases} \tag{7}$$

is the geodesic flow expressed by the embedded variables x and v, where $\alpha = \|v(0)\|$.

By details in [7] or Appendix A, dynamics B and O are solved as

$$B: \begin{cases} x(t) = x(0) \\ v(t) = \text{expm}\{-\Lambda(x(0))Ct\}v(0) \end{cases}, O: \begin{cases} x(t) = x(0) \\ v(t) = v(0) + \Lambda(x(0))\left[-\nabla_x U_{\mathcal{H}}(x(0))t + \mathcal{N}(0, 2Ct)\right] \end{cases},$$

where $U_{\mathcal{H}}(x) \triangleq -\log \pi_{\mathcal{H}}(x)$, expm$\{\cdot\}$ is the matrix exponent, and $\Lambda(x)$ is the projection onto the tangent space at x in the embedded manifold. For $\mathbb{R}^n$, $\Lambda(x) = I_n$ (the identity mapping in $\mathbb{R}^n$) and for $\mathbb{S}^{n-1}$ embedded in $\mathbb{R}^n$, $\Lambda(x) = I_n - xx^\top$ (see Appendix A.3).

We further reduce dynamics B for *scalar* C: $v(t) = \Lambda(x(0)) \exp\{-Ct\}v(0) = \exp\{-Ct\}v(0)$, by noting that $\exp\{-Ct\}$ is a scalar and $v(0)$ already lies on the tangent space at $x(0)$. To illustrate this form, we expand the exponent for small t and get $v(t) = (1 - Ct)v(0)$, which is exactly the action of a friction dissipating energy to control injected noise, as proposed in SGHMC. Our investigation reveals that this form holds generally for v as the momentum in the isometrically embedded space, but not the usual momentum p in the coordinate space. In SGHMC, v and p are undistinguishable, but in our case v can only lie in the tangent space and p is arbitrary in $\mathbb{R}^m$.

Integrator for gSGNHT We split dynamics (6) in a similar way:

$$A: \begin{cases} \mathrm{d}q = G^{-1}p\mathrm{d}t \\ \mathrm{d}p = -\frac{1}{2}\nabla_q\left[p^\top G^{-1}p\right]\mathrm{d}t \\ \mathrm{d}\xi = \left(\frac{1}{m}p^\top G^{-1}p - 1\right)\mathrm{d}t \end{cases}, B: \begin{cases} \mathrm{d}q = 0 \\ \mathrm{d}p = -\xi p\,\mathrm{d}t \\ \mathrm{d}\xi = 0 \end{cases}, O: \begin{cases} \mathrm{d}q = 0 \\ \mathrm{d}p = -\nabla_q U\mathrm{d}t - \frac{1}{2}\nabla_q \log|G|\,\mathrm{d}t \\ \qquad + \mathcal{N}(0, 2CG\mathrm{d}t) \\ \mathrm{d}\xi = 0 \end{cases}.$$

For dynamics A, the solution of q and p is again the geodesic flow. To solve ξ, we first figure out that for dynamics A, $p^\top G^{-1}p$ is constant: $\frac{\mathrm{d}}{\mathrm{d}t}\left[p^\top G(q)^{-1}p\right] = \nabla_q\left[p^\top G(q)^{-1}p\right]^\top \dot{q} + 2\left[G(q)^{-1}p\right]^\top \dot{p} = -2\dot{p}^\top\dot{q} + 2\dot{q}^\top\dot{p} = 0$. Alternatively we note that $\frac{1}{2}p^\top G^{-1}p = \frac{1}{2}v^\top v$ is the kinetic energy [3] conserved by motion with no force. Now the evolution of ξ can be solved as $\xi(t) = \xi(0) + \left(\frac{1}{m}v(0)^\top v(0) - 1\right)t$.

Dynamics O is identical to the one of SGGMC. Dynamics B can be solved similarly with only v updated: $v(t) = \exp\{-\xi(0)t\}v(0)$. Expansion of this recovers the dissipation of energy by an adaptive friction proposed by SGNHT, and we extend it to an embedded space.

Now we consider incorporating stochastic gradient. Only the common dynamics O is affected. Similar to Eqn. (1), we express the stochastic gradient as $\nabla_x \tilde{U}_{\mathcal{H}}(x) = \nabla_x U_{\mathcal{H}}(x) + \mathcal{N}(0, V(x))$, then reformulate the solution of dynamics O as

$$v(t) = v(0) + \Lambda(x(0)) \cdot \left[-\nabla_x \tilde{U}_{\mathcal{H}}(x(0))t + \mathcal{N}\left(0, 2Ct - V(x(0))t^2\right)\right]. \tag{8}$$

To estimate the usually unknown $V(x)$, a simple way is just to take it as zero, in the sense that $V(x)t^2$ is a higher order infinitesimal of $2Ct$ for t as a small simulation step size. Another way to estimate $V(x)$ is by the empirical Fisher information, as is done in [2].

Finally, as SSI suggests, we simulate the complete dynamics by exactly simulating these solutions alternately in an "ABOBA" pattern. For a time step size of ε, dynamics A and B advance by $\varepsilon/2$ for once and dynamics O by ε. As other SG-MCMCs, we omit the unscalable Metropolis-Hastings test. But the consistency is still guaranteed [8] of e.g. the estimation by averaging over samples drawn from SG-MCMCs. Algorithms of SGGMC and gSGNHT are listed in Appendix E.

4 Application to Spherical Admixture Model

We now apply SGGMC/gSGNHT to solve the challenging task of posterior inference in Spherical Admixture Model (SAM) [23]. SAM is a Bayesian topic model for spherical data (each datum is in some $\mathbb{S}^{d-1}$), such as the *tf-idf* representation of text data. It enables more feature representations for hierarchical Bayesian models, and have the benefit over Latent Dirichlet Allocation (LDA) [5] to directly model the absence of words. The structure of SAM is shown in Fig. 2. Each document v_d, each topic β_k, the corpus mean μ and the hyper-parameter m are all in $\mathbb{S}^{V-1}$ with V the vocabulary size. Each topic proportion θ_d is in $(K-1)$-dim simplex with K the number of topics.

[3] $p^\top G^{-1}p = (G^{-1}p)^\top G(G^{-1}p) = \dot{q}^\top(M^\top M)\dot{q} = (M\dot{q})^\top(M\dot{q}) = v^\top v$ for an isometric embedding.

SAM uses the von Mises-Fisher distribution (vMF) (see e.g. [20]) to model variables on hyperspheres. The vMF on $\mathbb{S}^{d-1}$ with mean $\mu \in \mathbb{S}^{d-1}$ and concentration parameter $\kappa \in \mathbb{R}^+$ has *pdf* (w.r.t the Hausdorff measure) $\text{vMF}(x|\mu,\kappa) = c_d(\kappa)\exp\{\kappa\mu^\top x\}$, where $c_d(\kappa) = \kappa^{d/2-1}/\big((2\pi)^{d/2}I_{d/2-1}(\kappa)\big)$ and $I_r(\cdot)$ denotes the modified Bessel function of the first kind and order r. Then the generating process of SAM is

- Draw $\mu \sim \text{vMF}(\mu|m,\kappa_0)$;
- For $k = 1,\dots,K$, draw topic $\beta_k \sim \text{vMF}(\beta_k|\mu,\sigma)$;
- For $d = 1,\dots,D$, draw $\theta_d \sim \text{Dir}(\theta_d|\alpha)$ and $v_d \sim \text{vMF}(v_d|\bar{v}(\beta,\theta_d),\kappa)$,

where $\bar{v}(\beta,\theta_d) \triangleq \frac{\beta\theta_d}{\|\beta\theta_d\|}$ with $\beta \triangleq (\beta_1,\dots,\beta_K)$ is an approximate spherical weighted mean of topics. The joint distribution of $\big(v \triangleq (v_1,\dots,v_D), \beta, \theta \triangleq (\theta_1,\dots,\theta_K), \mu\big)$ can be known.

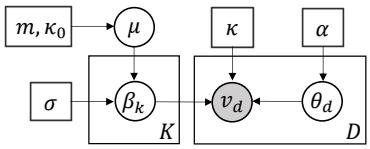

Figure 2: An illustration of SAM model structure.

The inference task is to estimate the topic posterior $\pi(\beta|v)$. As it is intractable, [23] provides a mean-field variational inference method and solves an optimization problem under spherical constraint, which is tackled by repeatedly normalizing. However, this treatment is not applicable to most sampling methods since it may corrupt the distribution of the samples. [23] tries a simple adaptive Metropolis-Hastings sampler with undesirable results, and no more attempt of sampling methods appears. Due to the deficiency of global coordinate system of hypersphere, most Riemann manifold samplers including SGRLD and SGRHMC fail. To our knowledge, only CHMC and GMC are suitable, yet not scalable. Our samplers are appropriate for the task, with the advantage of scalability.

Now we present our inference method that uses SGGMC/gSGNHT to directly sample from $\pi(\beta|v)$. First we note that μ can be collapsed analytically and the marginalized distribution of (v,β,θ) is:

$$\pi(v,\beta,\theta) = c_V(\kappa_0)c_V(\sigma)^K c_V(\|\bar{m}(\beta)\|)^{-1}\prod_{d=1}^{D}\text{Dir}(\theta_d|\alpha)\text{vMF}(v_d|\bar{v}(\beta,\theta_d),\kappa), \tag{9}$$

where $\bar{m}(\beta) \triangleq \kappa_0 m + \sigma\sum_{k=1}^K \beta_k$. To sample from $\pi(\beta|v)$ using our samplers, we only need to know a stochastic estimate of the gradient of potential energy $\nabla_\beta U(\beta|v) \triangleq -\nabla_\beta \log\pi(\beta|v)$, which can be estimated by adopting the technique used in [11]: $\nabla_\beta \log\pi(\beta|v) =$

$$\frac{1}{\pi(\beta|v)}\nabla_\beta\int\pi(\beta,\theta|v)\mathrm{d}\theta = \int\frac{\pi(\beta,\theta|v)}{\pi(\beta|v)}\frac{\nabla_\beta\pi(\beta,\theta|v)}{\pi(\beta,\theta|v)}\mathrm{d}\theta = \mathbb{E}_{\pi(\theta|\beta,v)}\left[\nabla_\beta\log\pi(\beta,\theta|v)\right],$$

where $\nabla_\beta\log\pi(\beta,\theta|v) = \nabla_\beta\log\pi(v,\beta,\theta)$ is known, and the expectation can be estimated by averaging over a set of samples $\{\theta^{(n)}\}_{n=1}^N$ from $\pi(\theta|v,\beta)$: $\nabla_\beta U(\beta|v) \approx \frac{1}{N}\sum_{n=1}^N \nabla_\beta\log\pi(v,\beta,\theta^{(n)})$. To draw $\{\theta^{(n)}\}_{n=1}^N$, noting the simplex constraint and that the target distribution $\pi(\theta|v,\beta)$ is known up to a constant multiplier, we use GMC to do the task.

To scale up, we use a subset $\{d(s)\}_{s=1}^S$ of indices of randomly chosen items from the whole data set to get a stochastic estimate for each $\nabla_\beta\log\pi(v,\beta,\theta^{(n)})$. The final stochastic gradient is:

$$\nabla_\beta\tilde{U}(\beta|v) \approx \nabla_\beta\log c_V(\|\bar{m}(\beta)\|) - \kappa\frac{D}{NS}\sum_{n=1}^N\sum_{s=1}^S v_{d(s)}^\top\bar{v}(\beta,\theta_{d(s)}^{(n)}). \tag{10}$$

The inference algorithm for SAM by SGGMC/gSGNHT is summarized in Alg. 3 in Appendix E.

5 Experiments

We present empirical results on both synthetic and real datasets to prove the accuracy and efficiency of our methods. All target densities are expressed in the embedded space w.r.t the Hausdorff measure so we omit the subscript "$\mathcal{H}$". Synthetic experiments are only for SGGMC since the advantage to use thermostats has been shown by [10] and the effectiveness of gSGNHT is presented on real datasets. Detailed settings of the experiments are provided in Appendix F.

5.1 Toy Experiment

We first present the utility and check the correctness of SGGMC by a greenhouse experiment with known stochastic gradient noise. Consider sampling from a circle ($\mathbb{S}^1$) for easy visualization. We set the target distribution such that the potential energy is $U(x) = -\log\big(\exp\{5\mu_1^\top x\} + 2\exp\{5\mu_2^\top x\}\big)$, where $x,\mu_1,\mu_2 \in \mathbb{S}^1$ and $\mu_1 = -\mu_2 = \frac{\pi}{3}$ (angle from $+x$ direction). The stochastic gradient is

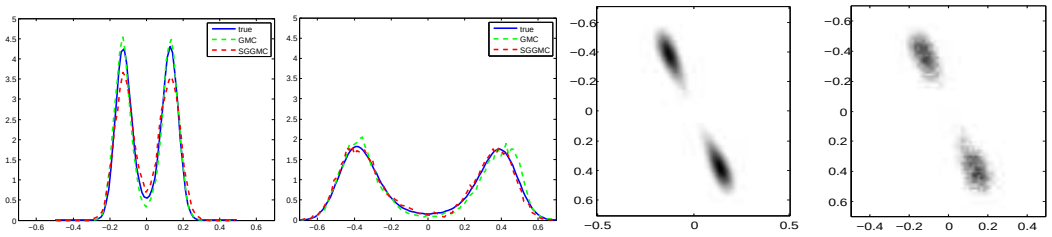

(a) $\pi(v_1|\mathcal{D})$ (b) $\pi(v_2|\mathcal{D})$ (c) $\pi(v_1, v_2|\mathcal{D})$

Figure 4: (a-b): True and empirical densities for $\pi(v_1|\mathcal{D})$ and $\pi(v_2|\mathcal{D})$. (c) True (left) and empirical by SGGMC (right) densities for $\pi(v_1, v_2|\mathcal{D})$.

produced by corrupting with $\mathcal{N}(0, 1000I)$, whose variance is used as $V(x)$ in Eqn. (8) for sampling. Fig. 3(a) shows 100 samples from SGGMC and empirical distribution of 10,000 samples in the embedded space $\mathbb{R}^2$. True and empirical distributions are compared in Fig. 3(b) in angle space (local coordinate space). We see no obvious corruption of the result when using stochastic gradient.

It should be stressed that although it is possible to apply scalable methods like SGRLD in spherical coordinate systems (almost global ones), it is too troublesome to work out the form of e.g. Riemann metric tensor, and special treatments like reflection at boundaries have to be considered. Numerical instability at boundaries also tends to appear. All these will get even worse in higher dimensions. Our methods work in embedded spaces, so all these issues are bypassed and can be elegantly extended to high dimensions.

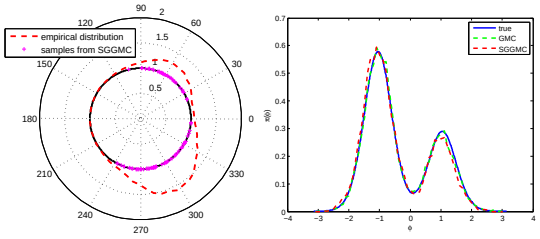

(a) samples by SGGMC in the embedded space (b) distribution comparison in angle space

Figure 3: Toy experiment results: (a) samples and empirical distribution of SGGMC; (b) comparison of true and empirical distributions.

5.2 Synthetic Experiment

We then test SGGMC on a simple Bayesian posterior estimation task. We adopt a model with similar structure as the one used in [28]. Consider a mixture model of two vMFs on $\mathbb{S}^1$ with equal weights:

$$\pi(v_1)=\text{vMF}(v_1|e_1,\kappa_1),\ \pi(v_2)=\text{vMF}(v_2|e_1,\kappa_2),\ \pi(x_i|v_1,v_2)\propto\text{vMF}(x_i|v_1,\kappa_x)+\text{vMF}(x_i|\mu,\kappa_x),$$

where $e_1 = (1, 0)$ and $\mu \triangleq (v_1 + v_2)/\|v_1 + v_2\|$. The task is to infer the posterior $\pi(v_1, v_2|\mathcal{D})$, where $\mathcal{D} = \{x_i\}_{i=1}^{D=100}$ is our synthetic data that is generated from the likelihood with $v_1 = -\frac{\pi}{24}, v_2 = \frac{\pi}{8}$ and $\kappa_1 = \kappa_2 = \kappa_x = 20$ by GMC. SGGMC uses empirical Fisher information in the way of [2] for $V(x)$ in Eqn. (8), and uses 10 for batch size. Fig. 4(a-b) show the true and empirical marginal posteriors of v_1 and v_2, and Fig. 4(c) presents empirical joint posterior by samples from SGGMC and its true density. We see that samples from SGGMC exhibit no observable corruption when a mini-batch is used, and fully explore the two modes and the strong correlation of v_1 and v_2. [4]

5.3 Spherical Admixture Models

Setups For baselines, we compare with the mean-field variational inference (**VI**) by [23] and its stochastic version (**StoVI**) based on [15], as well as GMC methods. It is problematic for GMC to directly sample from the target distribution $\pi(\beta|v)$ since the potential energy is hard to estimate, which is required for Metropolis-Hastings (MH) test in GMC. An approximate Monte Carlo estimation is provided in Appendix B and the corresponding method for SAM is **GMC-apprMH**. An alternative is **GMC-bGibbs**, which adopts blockwise Gibbs sampling to alternately sample from $\pi(\beta|\theta, v)$ and $\pi(\theta|\beta, v)$ (both known up to a constant multiplier) using GMC.

We evaluate the methods by *log-perplexity* — the average of negative log-likelihood on a held-out test set $\mathcal{D}_{test}$. Variational methods produce a single point estimate $\hat{\beta}$ and the log-perplexity is log-perp $= -\frac{1}{|\mathcal{D}_{test}|}\sum_{d\in\mathcal{D}_{test}}\log\pi(v_d|\hat{\beta})$. Sampling methods draw a set of samples $\{\beta^{(m)}\}_{m=1}^{M}$ and log-perp $= -\frac{1}{|\mathcal{D}_{test}|}\sum_{d\in\mathcal{D}_{test}}\log(\frac{1}{M}\sum_{m=1}^{M}\pi(v_d|\beta^{(m)}))$. In both cases the intractable $\pi(v_d|\beta)$ needs to be estimated. By noting that $\pi(v_d|\beta) = \int\pi(v_d, \theta_d|\beta)\text{d}\theta_d = \mathbb{E}_{\pi(\theta_d|\beta)}[\pi(v_d|\beta, \theta_d)]$, we

[4] Appendix D provides a rationale on the shape of the joint posterior.

estimate it by averaging $\pi(v_d|\beta, \theta_d^{(n)})$ (exactly known from the generating process) over samples $\{\theta_d^{(n)}\}_{n=1}^N$ drawn from $\pi(\theta_d|\beta) = \pi(\theta_d) = \text{Dir}(\alpha)$, the prior of θ_d. The log-perplexity is not comparable among different models so we exclude LDA from our baseline.

We show the performance of all methods on a small and a large dataset. Hyper-parameters of SAM are fixed while training and set the same for all methods. $V(x)$ in Eqn. (8) is taken zero for **SGGMC/gSGNHT**. All sampling methods are implemented [5] in C++ and *fairly* parallelized by OpenMP. **VI/StoVI** are run in MATLAB codes by [23] and we only use their final scores for comparison. Appendix F gives further implementation details, including techniques to avoid overflow.

On the small dataset The small dataset is the 20News-different dataset used by [23], which consists of 3 categories from 20Newsgroups dataset. It is small (1,666 training and 1,107 test documents) so we have the chance to see the eventual results of all methods. We use 20 topics and 50 as the batch size.

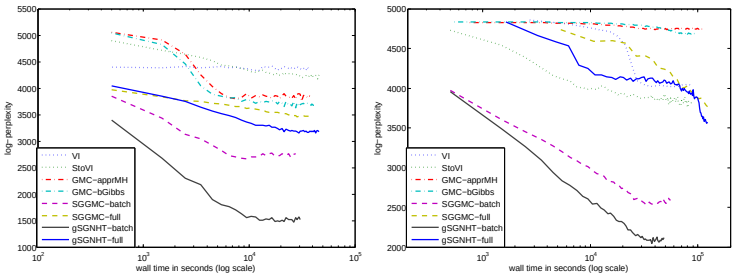

(a) 20News-different (b) 150K Wikipedia

Figure 5: Evolution of log-perplexity along wall time of all methods on (a) 20News-different dataset and (b) 150K Wikipedia subset.

Fig. 5(a) shows the performance of all methods. We can see that our **SGGMC** and **gSGNHT** perform better than others. **VI** converges swiftly but cannot go any lower due to the intrinsic gap between the mean-field variational distribution and the true posterior. **StoVI** converges slower than **VI** in this small scale case, and exhibits the same limit. All sampling methods eventually go below variational methods, and ours go the lowest. **gSGNHT** shows its benefit to outperform **SGGMC** under the same setting. For our methods, an appropriately smaller batch size achieves a better result due to the speed-up by subsampling. Note that even the full-batch **SGGMC** and **gSGNHT** outperform GMC variants. This may be due to the randomness in the dynamics helps jumping out of one local mode to another for a better exploration.

On the large dataset For the large dataset, we use a subset of the Wikipedia dataset with 150K training and 1K test documents, to challenge the scalability of all the methods. We use 50 topics and 100 as the batch size. Fig. 5(b) shows the outcome. We see that the gap between our methods and other baselines gets larger, indicating our scalability. Bounded curves of **VI/StoVI**, the advantage of using thermostats and subsampling speed-up appear again. Our full-batch versions are still better than GMC variants. **GMC-apprMH** and **GMC-bGibbs** scale badly; they converge slowly in this case.

6 Conclusions and Discussions

We propose SGGMC and gSGNHT, SG-MCMCs for scalable sampling from manifolds with known geodesic flow. They are saliently efficient on their applications. Novel dynamics are constructed and 2nd-order geodesic integrators are developed. We apply the methods to SAM topic model for more accurate and scalable inference. Synthetic experiments verify the validity and experiments for SAM on real-world data shows an obvious advantage in accuracy over variational inference methods and in scalability over other applicable sampling methods. There remains possible broad applications of our methods, including models involving vMF (e.g. mixture of vMF [4, 14, 27], DP mixture of vMF [12, 3, 26]), constraint distributions [17] (e.g. truncated Gaussian), and distributions on Stiefel manifold (e.g. Bayesian matrix completion [24]), where the ability of scale-up will be appealing.

Acknowledgments

The work was supported by the National Basic Research Program (973 Program) of China (No. 2013CB329403), National NSF of China Projects (Nos. 61620106010, 61322308, 61332007), the Youth Top-notch Talent Support Program, and Tsinghua Initiative Scientific Research Program (No. 20141080934).

[5] All the codes and data can be found at `http://ml.cs.tsinghua.edu.cn/~changliu/sggmcmc-sam/`.

References

[1] Ralph Abraham, Jerrold E Marsden, and Jerrold E Marsden. *Foundations of mechanics*. Benjamin/Cummings Publishing Company Reading, Massachusetts, 1978.

[2] Sungjin Ahn, Anoop Korattikara, and Max Welling. Bayesian posterior sampling via stochastic gradient fisher scoring. *arXiv preprint arXiv:1206.6380*, 2012.

[3] Nguyen Kim Anh, Nguyen The Tam, and Ngo Van Linh. Document clustering using dirichlet process mixture model of von mises-fisher distributions. In *The 4th International Symposium on Information and Communication Technology, SoICT 2013*, page 131–138, 2013.

[4] Arindam Banerjee, Inderjit S Dhillon, Joydeep Ghosh, and Suvrit Sra. Clustering on the unit hypersphere using von mises-fisher distributions. *Journal of Machine Learning Research*, 6:1345–1382, 2005.

[5] David M. Blei, Andrew Y. Ng, and Michael I. Jordan. Latent dirichlet allocation. *The Journal of Machine Learning Research*, 3:993–1022, 2003.

[6] Marcus A. Brubaker, Mathieu Salzmann, and Raquel Urtasun. A family of mcmc methods on implicitly defined manifolds. In *Proceedings of the 15th International Conference on Artificial Intelligence and Statistics (AISTATS)*, pages 161–172, 2012.

[7] Simon Byrne and Mark Girolami. Geodesic monte carlo on embedded manifolds. *Scandinavian Journal of Statistics*, 40(4):825–845, 2013.

[8] Changyou Chen, Nan Ding, and Lawrence Carin. On the convergence of stochastic gradient mcmc algorithms with high-order integrators. In *Advances in Neural Information Processing Systems*, pages 2269–2277, 2015.

[9] Tianqi Chen, Emily Fox, and Carlos Guestrin. Stochastic gradient hamiltonian monte carlo. In *Proceedings of the 31st International Conference on Machine Learning (ICML-14)*, pages 1683–1691, 2014.

[10] Nan Ding, Youhan Fang, Ryan Babbush, Changyou Chen, Robert D. Skeel, and Hartmut Neven. Bayesian sampling using stochastic gradient thermostats. In *Advances in Neural Information Processing Systems*, pages 3203–3211, 2014.

[11] Chao Du, Jun Zhu, and Bo Zhang. Learning deep generative models with doubly stochastic mcmc. *arXiv preprint arXiv:1506.04557*, 2015.

[12] Kaushik Ghosh, Rao Jammalamadaka, and Ram C. Tiwari. Semiparametric bayesian techniques for problems in circular data. *Journal of Applied Statistics*, 30(2):145–161, 2003.

[13] Mark Girolami and Ben Calderhead. Riemann manifold langevin and hamiltonian monte carlo methods. *Journal of the Royal Statistical Society: Series B (Statistical Methodology)*, 73(2):123–214, 2011.

[14] Siddharth Gopal and Yiming Yang. Von mises-fisher clustering models. In *Proceedings of the 31st International Conference on Machine Learning (ICML-14)*, 2014.

[15] Matthew D. Hoffman, David M. Blei, Chong Wang, and John Paisley. Stochastic variational inference. *The Journal of Machine Learning Research*, 14(1):1303–1347, 2013.

[16] I. M. James. *The topology of Stiefel manifolds*, volume 24. Cambridge University Press, 1976.

[17] Shiwei Lan, Bo Zhou, and Babak Shahbaba. Spherical hamiltonian monte carlo for constrained target distributions. In *Proceedings of the 31st International Conference on Machine Learning (ICML-14)*, pages 629–637, 2014.

[18] Chunyuan Li, Changyou Chen, Kai Fan, and Lawrence Carin. High-order stochastic gradient thermostats for bayesian learning of deep models. *arXiv preprint arXiv:1512.07662*, 2015.

[19] Yi-An Ma, Tianqi Chen, and Emily Fox. A complete recipe for stochastic gradient mcmc. In *Advances in Neural Information Processing Systems*, pages 2899–2907, 2015.

[20] Kanti V. Mardia and Peter E. Jupp. Distributions on spheres. *Directional Statistics*, pages 159–192, 2000.

[21] Radford M. Neal. Mcmc using hamiltonian dynamics. *Handbook of Markov Chain Monte Carlo*, 2, 2011.

[22] Sam Patterson and Yee Whye Teh. Stochastic gradient riemannian langevin dynamics on the probability simplex. In *Advances in Neural Information Processing Systems*, pages 3102–3110, 2013.

[23] Joseph Reisinger, Austin Waters, Bryan Silverthorn, and Raymond J. Mooney. Spherical topic models. In *Proceedings of the 27th International Conference on Machine Learning (ICML-10)*, pages 903–910, 2010.

[24] Yang Song and Jun Zhu. Bayesian matrix completion via adaptive relaxed spectral regularization. In *The 30th AAAI Conference on Artificial Intelligence (AAAI-16)*, 2016.

[25] Eduard L. Stiefel. Richtungsfelder und fernparallelismus in n-dimensionalen mannigfaltigkeiten. *Commentarii Mathematici Helvetici*, 8(1):305–353, 1935.

[26] Julian Straub, Jason Chang, Oren Freifeld, and John W. Fisher III. A dirichlet process mixture model for spherical data. In *Proceedings of the 18th International Conference on Artificial Intelligence and Statistics (AISTATS)*, pages 930–938, 2015.

[27] Jalil Taghia, Zhanyu Ma, and Arne Leijon. Bayesian estimation of the von mises-fisher mixture model with variational inference. *IEEE Transactions on Pattern Analysis and Machine Intelligence*, 36(9):1701–1715, 2014.

[28] Max Welling and Yee Whye Teh. Bayesian learning via stochastic gradient langevin dynamics. In *Proceedings of the 28th International Conference on Machine Learning (ICML-11)*, pages 681–688, 2011.

Supplementary Material for: Stochastic Gradient Geodesic MCMC Methods

Chang Liu[†], **Jun Zhu**[†], **Yang Song**[‡*]
[†] Dept. of Comp. Sci. & Tech., TNList Lab; Center for Bio-Inspired Computing Research
[†] State Key Lab for Intell. Tech. & Systems, Tsinghua University, Beijing, China
[‡] Dept. of Physics, Tsinghua University, Beijing, China
{chang-li14@mails, dcszj@}.tsinghua.edu.cn; songyang@stanford.edu

Appendix A: Details for Solving Dynamics B and O in the Embedded Space

In this section, we present details used in Sec. 3.3 of the main paper to solve dynamics B and O in the embedded space for releasing local coordinate systems and a cheap simulation rule. We only show the details for SGGMC, and the procedure is quite similar for gSGNHT. The technique is adapted from [2], and we reformulate it here for completeness and easier comprehension.

A.1: Main Details

Dynamics B and O of SGGMC in the coordinate space (see Sec. 3.3.1 of the main paper) are:

$$B:\begin{cases}\mathrm{d}q=0\\ \mathrm{d}p=-M^\top CMG^{-1}p\,\mathrm{d}t\end{cases},O:\begin{cases}\mathrm{d}q=0\\ \mathrm{d}p=-\nabla_q U(q)\,\mathrm{d}t-\frac{1}{2}\nabla_q\log|G(q)|\,\mathrm{d}t+\mathcal{N}(0,2M^\top CM\mathrm{d}t)\end{cases}.$$

We do the transformation into the embedded space based on the map $x=\xi(q)$. Note that for both dynamics, q is constant so $\dot{x}=(\nabla_q\xi)^\top\dot{q}=0$. From dynamics A in Sec. 3.3.1 (or the definition of momentum in Appendix C), we have $p=G(q)\dot{q}$ and by some calculus we have $\nabla_q=M^\top\nabla_x$. From Sec. 3.1 we have $\pi_{\mathcal{H}}(x)=\pi(q)/\sqrt{|G(q)|}$ and $U_{\mathcal{H}}(x)\triangleq-\log\pi_{\mathcal{H}}(x)=U(q)+\frac{1}{2}\log|G(q)|$. So we have

$$B:\begin{cases}\mathrm{d}x=0\\ G(q)\mathrm{d}\dot{q}=-M^\top CM\dot{q}\,\mathrm{d}t\end{cases},O:\begin{cases}\mathrm{d}x=0\\ G(q)\mathrm{d}\dot{q}=-M^\top\nabla_x U_{\mathcal{H}}(x)\mathrm{d}t+M^\top\mathcal{N}(0,2C\mathrm{d}t)\end{cases}.$$

We then left multiply $M(q)G(q)^{-1}$ for both momentum equations and have

$$B:\begin{cases}\mathrm{d}x=0\\ \mathrm{d}(M\dot{q})=-MG(q)^{-1}M^\top CM\dot{q}\,\mathrm{d}t\end{cases},O:\begin{cases}\mathrm{d}x=0\\ \mathrm{d}(M\dot{q})=-MG(q)^{-1}M^\top\nabla_x U_{\mathcal{H}}(x)\mathrm{d}t\\ \qquad\qquad+MG(q)^{-1}M^\top\mathcal{N}(0,2C\mathrm{d}t)\end{cases}.$$

By definition $v\triangleq\dot{x}=M\dot{q}$; from the isometric property of the Riemann metric $G(q)$, we have $G=M^\top M$. So finally we have

$$B:\begin{cases}\mathrm{d}x=0\\ \mathrm{d}v=-M(M^\top M)^{-1}M^\top Cv\,\mathrm{d}t\end{cases},O:\begin{cases}\mathrm{d}x=0\\ \mathrm{d}v=M(M^\top M)^{-1}M^\top\Big(-\nabla_x U_{\mathcal{H}}(x)\mathrm{d}t+\mathcal{N}(0,2C\mathrm{d}t)\Big)\end{cases}.$$

We can write $M(x)=M(\xi^{-1}(x))$ so M can be expressed in the embedded space. Now we complete the transformation into the embedded space.

*JZ is the corresponding author; YS is with Department of Computer Science, Stanford University, CA.

29th Conference on Neural Information Processing Systems (NIPS 2016), Barcelona, Spain.

Note that the matrix $M(M^\top M)^{-1}M^\top$, which we denote as $\Lambda(x)$, is the orthogonal projection onto the column space of M (see Appendix A.2), which is $T_x(\Xi(\mathcal{M}))$, the tangent space of the embedded manifold at x (a conclusion from differential geometry). [2] proposes an alternative expression for $\Lambda(x)$ that can be more intuitively constructed and is computationally cheaper. Appendix A.2 shows the interpretation of the two expressions and Appendix A.3 derives $\Lambda(x)$ for hyperspheres based on both expressions. By noting that x is constant for both dynamics, we can analytically solve them

$$B:\begin{cases} x(t) =& x(0) \\ v(t) =& \text{expm}\left\{-\Lambda\big(x(0)\big)Ct\right\} v(0) \end{cases}, O:\begin{cases} x(t)=&x(0) \\ v(t)=&v(0)+\Lambda\big(x(0)\big)\big[-\nabla_x U_{\mathcal{H}}\big(x(0)\big)t+\mathcal{N}(0,2Ct)\big] \end{cases}$$

as given in the main paper.

A.2: Interpretation of the Two Expressions of the Orthogonal Projection $\Lambda(x)$

We first interpret that $\Lambda(x) \triangleq M(M^\top M)^{-1}M^\top$ is an orthogonal projection onto the column space $C(M)$ of M. In our case, $M_{n\times m}$ has full column rank (differential geometry conclusion) so $C(M)$ is an m-dim subspace (hyperplane) of $\mathbb{R}^n$. An orthogonal projection of $x \in \mathbb{R}^n$ onto $C(M)$ gives the following decomposition

$$x = y + z,$$

where $y \in C(M)$, $z \in (C(M))^\perp$ so $y^\top z = 0$. Express y as $y = M\theta_x$, where $\theta \in \mathbb{R}^m$ acts as the coordinate of elements in $C(M)$. Then $y^\top z = 0$ gives $(M\theta_x)^\top(x - M\theta_x) = 0$, which is $\theta_x^\top(M^\top x - M^\top M\theta_x) = 0$, and we solve

$$\theta_x = (M^\top M)^{-1}M^\top x.$$

So $y = M(M^\top M)^{-1}M^\top x$, revealing the meaning of $\Lambda(x)$ as the orthogonal projection onto $C(M)$.

Now we introduce another expression for $\Lambda(x)$ proposed in [2]. Let $N_{n\times(n-m)}$ be a set of orthonormal basis (collected in columns) of $(C(M))^\perp$ so that $N^\top N = I_{n-m}$. Express z as $z = N\phi_x$, where $\phi \in \mathbb{R}^{n-m}$ acts as the coordinate of elements in $(C(M))^\perp$. Then $y^\top z = 0$ gives $(N\phi_x)^\top(x - N\phi_x) = 0$, and we solve

$$\phi_x = (N^\top N)^{-1}N^\top x = N^\top x.$$

So $y = x - NN^\top x$, revealing the meaning of $I_n - NN^\top$ as the same projection. This expression is proposed because N is usually more sensible, especially for hyperspheres as shown in Appendix A.3. It also saves computation since only one thin matrix multiplication is required, instead of more than three matrix multiplications and possibly a matrix inversion for the former expression.

A.3: A Derivation of the Projection $\Lambda(x)$ for the Hypersphere Example

First we need to describe a hypersphere in depth. A $(d-1)$-dim hypersphere $\mathbb{S}^{d-1} \triangleq \{x \in \mathbb{R}^d | \|x\| = 1\}$ is defined as a subset of $\mathbb{R}^n$, so we can *isometrically* embed it into $\mathbb{R}^d$ by an identity mapping $\Xi : \mathbb{S}^{d-1} \to \mathbb{R}^d, x \mapsto x$. To get $M(q)$, we need to specify a local coordinate system for $\mathbb{S}^{d-1}$. We select $\mathcal{N} = \{x \in \mathbb{S}^{d-1} | x_d > 0\}$ i.e. the upper semi-hypersphere, and $\Omega = \{q = (q_1, \ldots, q_{d-1})^\top | \sum_{i=1}^{d-1} q_i^2 < 1\} \subset \mathbb{R}^{d-1}$. For $x \in \mathcal{N}$, define $\Phi(x) = (x_1, \ldots, x_{d-1})^\top \in \Omega$. Then $(\mathcal{N}, \Phi)$ is a local coordinate system for $\mathbb{S}^{d-1}$ and $\xi(q) = (q_1, \ldots, q_{d-1}, \xi_d)^\top \in \mathbb{R}^d$, where $\xi_d = \sqrt{1 - \sum_{i=1}^{d-1} q_i^2}$. By definition, we have

$$M(q) = \begin{pmatrix} I_{d-1} \\ -q^\top/\xi_d \end{pmatrix}, G(q) = M^\top M = I_{d-1} + \frac{qq^\top}{\xi_d^2}.$$

By the Sherman-Morrison formula, we have

$$G(q)^{-1} = I_{d-1} - qq^\top.$$

So according to the first expression of $\Lambda(x)$, we have

$$\Lambda(\xi(q)) = MG^{-1}M^\top = \begin{pmatrix} I_{d-1} - qq^\top & -\xi_d q \\ -\xi_d q^\top & 1 - \xi_d^2 \end{pmatrix} = I_d - \xi(q)\xi(q)^\top,$$

or $\Lambda(x) = I_d - xx^\top, x \in \Xi(\mathcal{N})$. We successively select similar local coordinate systems (i.e. select Ω as lower semi-hypersphere, east semi-hypersphere, etc.) until $\mathbb{S}^{d-1}$ can be covered by these coordinates. For each of these local coordinate systems, we have the same conclusion. To sum up, we have $\Lambda(x) = I_d - xx^\top, x \in \Xi(\mathcal{M})$.

Another way to implement the projection is though the orthonormal basis $N(x)_{n\times(n-m)}$ of the orthogonal complement of the tangent space. For the hypersphere $\mathbb{S}^{d-1}$, the tangent space $T_x\mathbb{S}^{d-1}$ is intuitively a $(d-1)$-dim subplane in $\mathbb{R}^d$ perpendicular to the direction of radius, which is just x. The orthogonal complement of the plane is the line in the direction of x. Thus $N(x) = x$ and by the second expression $\Lambda(x) = I_d - xx^\top$, the same as derived by the first expression. We see that this derivation is more neat.

Appendix B: Estimation of the Potential Energy $U(\beta|v)$ for SAM

For the SAM inference task, the potential energy $U(\beta|v) \triangleq -\log\pi(\beta|v)$ is required for GMC to directly sample from $\pi(\beta|v)$. It is involved since we do not know the closed form of $U(\beta|v)$, even ignoring a shifting constant. By referring to the unbiased Monte Carlo estimation of its gradient $-\nabla_\beta \log\pi(\beta|v) = -\mathbb{E}_{\pi(\theta|v,\beta)}\left[\nabla_\beta \log\pi(\beta,\theta|v)\right]$ as provided in Sec. 4 of the main paper, one possible estimation can be formed by samples $\{\theta^{(n)}\}_{n=1}^N$ from $\pi(\theta|v,\beta)$:

$$U(\beta|v) \approx -\frac{1}{N}\sum_{n=1}^{N} \log\pi(\beta,\theta^{(n)}|v) + \text{const.} \tag{1}$$

Unfortunately, this estimation is biased. The relation between the estimation and the true value can be found by

$$\begin{aligned} U(\beta|v) &= -\mathbb{E}_{\pi(\theta|v,\beta)}\left[\log\pi(\beta|v)\right] \qquad \text{(since } \log\pi(\beta|v) \text{ is independent of } \theta\text{)} \\ &= -\mathbb{E}_{\pi(\theta|v,\beta)}\left[\log\pi(\beta,\theta|v) - \log\pi(\theta|v,\beta)\right] \\ &\approx -\frac{1}{N}\sum_{n=1}^{N}\Big(\log\pi(\beta,\theta^{(n)}|v) - \log\pi(\theta^{(n)}|v,\beta)\Big), \end{aligned}$$

where an average of $-\log\pi(\theta^{(n)}|v,\beta)$ lies between them. Although $\log\pi(\theta|v,\beta)$ is known up to a shifting constant, it cannot meet the demand here since the θ-free shifting constant varies with β, and we consider a function of β here.

Nevertheless Eqn. (1) seems to be the only way to estimate the potential energy. It can be used by an approximation: when the proposal of β is not distant from its beginning value, $\pi(\theta|v,\beta)$ does not change much. Adopting this, a sampling inference method for SAM by directly sample from $\pi(\beta|v)$ can be conceived, i.e. **GMC-apprMH**. The gradient is estimated in the same way as **SGGMC** except it uses the whole dataset.

Due to the inaccuracy of this, **GMC-bGibbs** is considered. But **GMC-apprMH** is in the same scheme of **SGGMC/gSGNHT** since they draw one sample of β based on multiple samples of θ, while **GMC-bGibbs** only use one sample of θ for each β.

Appendix C: A Derivation of the Momentum and the Hamiltonian Originated from Physics

In classical mechanics (see e.g. [5]), there is a formal derivation for the Hamiltonian, beginning with the Lagrangian. In the coordinate space, the Lagrangian is defined by $L(q,\dot{q}) = \frac{1}{2}\dot{q}^\top G(q)\dot{q} - U_{\mathcal{H}}\big(\xi(q)\big)$, where $q \in \Omega$ and $\dot{q} \in T_q\Omega = \mathbb{R}^m$. The Hamiltonian is defined as the Legendre transformation of the Lagrangian $L(q,\dot{q})$. To perform the transformation, define the (generalized conjugate) momentum as $p \triangleq \frac{\partial L}{\partial \dot{q}} = G(q)\dot{q}$, and accordingly express $\dot{q} = \dot{q}(q,p) = G(q)^{-1}p$, then the Hamiltonian is expressed as

$$H(z) \triangleq \Big(p^\top\dot{q} - L(q,\dot{q})\Big)\Big|_{\dot{q}=\dot{q}(q,p)} = \frac{1}{2}p^\top G(q)^{-1}p + U_{\mathcal{H}}\big(\xi(q)\big),$$

where $z \triangleq (q,p)$ is called the canonical coordinates. This is the same as the one used by SGGMC.

In an isometrically embedded space, the same procedure can be applied. The Lagrangian now is $L(x, \dot{x}) = \frac{1}{2}\dot{x}^\top \dot{x} - U_{\mathcal{H}}(x)$, where $x \in \Xi(\mathcal{M})$ and $\dot{x} \in T_x\Xi(\mathcal{M})$ (the tangent space of $\Xi(\mathcal{M})$ at x). The momentum in the embedded space is thus $v \triangleq \frac{\partial L}{\partial \dot{x}} = \dot{x}$. The Hamiltonian is derived by

$$H(x, v) \triangleq \left(x^\top \dot{x} - L(x, \dot{x})\right)\Big|_{\dot{x}=\dot{x}(x,v)} = \frac{1}{2}v^\top v + U_{\mathcal{H}}(x).$$

This is the common form of the Hamiltonian, where the "velocity" should be regarded as the momentum in the isometrically embedded space for a general case.

Appendix D: A Rationale on the Shape of the Joint Posterior for the Synthetic Experiment

In this part we provide an interpretation for the symmetric bimodal shape of the posterior $\pi(v_1, v_2|\mathcal{D})$ for the simple mixture of vMF model in Sec. 5.2 of the main paper. We start with the way we generate the synthetic data. They are samples drawn by GMC from the likelihood $\pi(x_i|v_1, v_2) \propto \text{vMF}(x_i|v_1, \kappa_x) + \text{vMF}(x_i|\mu, \kappa_x)$, with $\mu \triangleq (v_1 + v_2)/\|v_1 + v_2\|$, and $v_1 = v_1^{(g)}$ and $v_2 = v_2^{(g)}$ as shown in Fig. 1 (left). Due to the mono-modal shape of vMF, the synthetic data has two modes: $v_1^{(g)}$ and $\mu^{(g)}$. On the other hand, by referring to the generating process, the modes of x are v_1 and μ. Thus, we can approximately (under a weak prior) estimate the modes of the posterior by matching the theoretical data modes and the observed data modes: 1) let $v_1 = v_1^{(g)}, \mu = \mu^{(g)}$, we have $v_1^{(1)} = v_1^{(g)}, v_2^{(1)} = v_2^{(g)}$, i.e. the value used to generate data; 2) let $v_1 = \mu^{(g)}, \mu = v_1^{(g)}$, we have $v_1^{(2)} = \mu^{(g)}$ and $v_2^{(2)}$ shown in Fig. 1 (right). Note that the two approximate modes of the posterior are symmetric with respect to e_1, so they share equal preference from the prior. In our settings $\phi = \frac{\pi}{6}$, so we expect the posterior to have two equal-weighted modes around $(-\frac{\pi}{24}, \frac{\pi}{8})$ and $(\frac{\pi}{24}, -\frac{\pi}{8})$. Our experiment results in the main paper meets this reasoning.

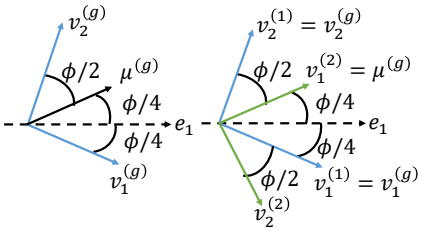

Figure 1: Left plot shows v_1, v_2, μ for generating data. Modes of the synthetic data are $v_1^{(g)}$ and $\mu^{(g)}$. Right plot shows the two approximate modes of the posterior under a weak prior: $(v_1^{(1)}, v_2^{(1)})$ in blue and $(v_1^{(2)}, v_2^{(2)})$ in green.

Appendix E: Algorithms of SGGMC/gSGNHT and their application to SAM

Based on the statements in Sec. 3.3 of the main paper, we summarize the algorithms of our proposed SGGMC and gSGNHT in Alg. 1 and Alg. 2, respectively. Here we only present algorithms for *scalar* C.

For both SGGMC and gSGNHT, the step size schedule $\{\varepsilon_n\}$ is recommended to be a fixed number. Although a shrinking schedule, e.g. $\varepsilon_n \propto n^{-k}$ for $k \in (0, 1)$ mentioned in [3], enjoys more theoretical guarantees (sample average is asymptotically unbiased even if the stochastic gradient may not be unbiased [3]), but the advantage may not show up in practice and the performance may be affected by insufficient exploration.

The first two parameters of our SGGMC/gSGNHT, the fixed step size ε and the scalar C, can be managed in a similar way of SGHMC [4], which utilizes its analogy to stochastic gradient descent (SGD) with momentum. By introducing two SGD terminologies, the per-batch learning rate γ and the coefficient of momentum ρ (both scalar), our parameters can be set as $\varepsilon = \sqrt{\gamma/|\mathcal{D}|}$ and $C = \rho/\varepsilon$. Typical values of γ and ρ are around 0.1 to 0.01. The last parameter is the number of steps L. For SG-MCMCs it is often set to 1, in the sense that L does not affect the simulation trajectory, different from HMC. Other integers can also be used, with less correlated samples. Automatic selection of L for SG-MCMCs remains to be studied, while the counterpart for HMC is provided as the No-U-Turn Sampler (NUTS) [6].

From the contents in Sec. 4 of the main paper, the algorithm to use SGGMC/gSGNHT for the inference problem of SAM is presented in Alg. 3.

Algorithm 1 Sampling procedure of SGGMC

Randomly initialize $x^{(0)} \in \Xi(\mathcal{M})$.
Sample $v^* \sim \mathcal{N}(0, I)$ and project $v^{(0)} \leftarrow \Lambda(x^{(0)})v^*$.
for $n = 1, 2, \ldots,$ **do**
  Sample a subset $\mathcal{S}$ for computing $\nabla_x \tilde{U}_{\mathcal{H}}(x)$. $(x_0, v_0) \leftarrow (x^{(n-1)}, v^{(n-1)})$.
  for $l = 1, 2, \ldots, L$ **do**
    A: Update $(x^*, v^*) \leftarrow (x_{l-1}, v_{l-1})$ by the geodesic flow for time step $\frac{\varepsilon_n}{2}$.
    B: $v^* \leftarrow \exp\{-C\frac{\varepsilon_n}{2}\}v^*$.
    O: $v^* \leftarrow v^* + \Lambda(x^*) \cdot \Big[-\nabla_x \tilde{U}_{\mathcal{H}}(x^*)\varepsilon_n + \mathcal{N}\big(0, (2C - \varepsilon_n V(x^*))\varepsilon_n\big)\Big]$.
    B: $v^* \leftarrow \exp\{-C\frac{\varepsilon_n}{2}\}v^*$.
    A: Update $(x_l, v_l) \leftarrow (x^*, v^*)$ by the geodesic flow for time step $\frac{\varepsilon_n}{2}$.
  end for
  $(x^{(n+1)}, v^{(n+1)}) \leftarrow (x_L, v_L)$. No M-H test.
end for

Algorithm 2 Sampling procedure of gSGNHT

Randomly initialize $x^{(0)} \in \Xi(\mathcal{M})$.
Sample $v^* \sim \mathcal{N}(0, I)$ and project $v^{(0)} \leftarrow \Lambda(x^{(0)})v^*$. $\xi^{(0)} \leftarrow C$.
for $n = 1, 2, \ldots,$ **do**
  Sample a subset $\mathcal{S}$ for computing $\nabla_x \tilde{U}_{\mathcal{H}}(x)$. $(x_0, v_0, \xi_0) \leftarrow (x^{(n-1)}, v^{(n-1)}, \xi^{(n-1)})$.
  for $l = 1, 2, \ldots, L$ **do**
    A: Update $(x^*, v^*) \leftarrow (x_{l-1}, v_{l-1})$ by the geodesic flow for time step $\frac{\varepsilon_n}{2}$,
      $\xi^* \leftarrow \xi_{l-1} + (\frac{1}{m} v_{l-1}^\top v_{l-1} - 1)\frac{\varepsilon_n}{2}$.
    B: $v^* \leftarrow \exp\{-\xi^*\frac{\varepsilon_n}{2}\}v^*$.
    O: $v^* \leftarrow v^* + \Lambda(x^*) \cdot \Big[-\nabla_x \tilde{U}_{\mathcal{H}}(x^*)\varepsilon_n + \mathcal{N}\big(0, (2C - \varepsilon_n V(x^*))\varepsilon_n\big)\Big]$.
    B: $v^* \leftarrow \exp\{-\xi^*\frac{\varepsilon_n}{2}\}v^*$.
    A: Update $(x_l, v_l) \leftarrow (x^*, v^*)$ by the geodesic flow for time step $\frac{\varepsilon_n}{2}$,
      $\xi_l \leftarrow \xi^* + (\frac{1}{m} {v^*}^\top v^* - 1)\frac{\varepsilon_n}{2}$.
  end for
  $(x^{(n)}, v^{(n)}, \xi^{(n)}) \leftarrow (x_L, v_L, \xi_L)$. No M-H test.
end for

Appendix F: Implementation Details for Experiments

F.1: Toy experiment in Sec. 5.1.

To draw 10,000 samples by each method, we set $L = 30$, $\varepsilon = 1 \times 10^{-2}$ for both GMC and SGGMC, and $\rho = 0.1$ for SGGMC. For the empirical distribution, the bin size is set to 0.1.

F.2: Synthetic experiment in Sec. 5.2.

The 100-sized synthetic data is generated by GMC without burn-in. To draw from the posterior, we set $L = 20$ and $\varepsilon = 1 \times 10^{-3}$ for GMC, and $L = 10$, $\rho = 0.1$ and $\gamma = 5 \times 10^{-4}$ for SGGMC. For each method, 25,000 posterior samples are taken after 15,000 burned in.

F.3: Spherical admixture model experiment in Sec. 5.3.

The two datasets and codes for all inference methods are available at `http://ml.cs.tsinghua.edu.cn/~changliu/sggmcmc-sam/`.

Datasets Both datasets present the *term frequency-inverse document frequency*, or *tf-idf* feature of documents. They are converted from the *bag-of-words* feature of their corresponding original datasets, which provide *tf*(d, v) — term frequency (number of occurrence) of term v in document d. The conversion is done by first computing *tf-idf*$(d, v) =$ *tf*$(d, v) \cdot \log\big(D/(1 +$ *df*$(v))\big)$, where D is the number of documents in the dataset, and *df*(v) is the document frequency of term v (number of

Algorithm 3 sampling inference for SAM using SGGMC/gSGNHT

for $m = 1, 2, \ldots$ **do**
  Randomly sample a subset $\{d(s)\}_{s=1}^{S}$ from whole training data.
  for $s = 1, 2, \ldots, S$ **do**
    Sample N times from $\pi(\theta_{d(s)}|\beta^{(m-1)}, v_{d(s)})$ using GMC to get $\{\theta_{d(s)}^{(n)}\}_{n=1}^{N}$.
  end for
  Sample once from $\pi(\beta|v)$ using SGGMC/gSGNHT to get $\beta^{(m)}$, with stochastic gradient computed by Eqn. (10) in the main paper.
end for

documents containing term v), then ℓ_2-normalizing the vector with component v equal to *tf-idf*(d, v) for a fixed d and getting the unit vector *tf-idf*(d) for document d.

The small dataset 20News-different is a subset of the 20Newsgroups dataset (`http://www.qwone.com/~jason/20Newsgroups/`, we use the Matlab/Octave version). It contains 3 categories out of the total 20: *rec.sport.baseball*, *sci.space* and *alt.atheism*. It is used by [8] to illustrate the benefits of SAM over LDA [1] in feature reduction. The original vocabulary size is 61,188, and we shrink it to 5,000 by selecting words with moderate document frequency (between 0.36% and 11.77%). While training by any method on the dataset, hyper-parameters of SAM are fixed as $\sigma = 1 \times 10^4$, $\kappa_0 = 1 \times 10^4$, $\kappa_1 = 3 \times 10^4$, $\alpha = 10$, and m set to the normalized mean of training documents.

The large dataset is based on the 6.6M Wikipedia dataset used by [9] (`http://ml.cs.tsinghua.edu.cn/~aonan/datasets/wikipedia/`). The original vocabulary size is 7,702, and we shrink it to 3,000 by selecting words with moderate document frequency (between 0.44% and 5.99%). Our dataset is then generated by randomly (excluding documents with ≤ 20 words) choosing 150K training and 1K test documents from the 6.6M whole dataset. The training size is the same as used by [7] for presenting scalability. While training by any method on the dataset, hyper-parameters of SAM are fixed as $\sigma = 6 \times 10^3$, $\kappa_0 = 6 \times 10^3$, $\kappa_1 = 2 \times 10^4$, $\alpha = 10$, and m set to the normalized mean of training documents.

Issues on the sampling methods For all sampling methods, samples of topic proportion θ_d of document d drawn from $\pi(\theta_d|v_d, \beta)$ are required. This can be well done by GMC. We use the initialization $\theta_d = (\beta^\top\beta)^{-1}\beta^\top v_d$ for sampling θ_d, which is the mode of $\pi(\theta_d|v_d, \beta)$ under an uninformative prior $\alpha = 1$. For **GMC-apprMH/GMC-bGibbs**, to draw one sample of β, sampling θ_d are carried out for all the documents in the training data, while **SGGMC/gSGNHT** only need to traverse the chosen mini-batch. Noting that drawing θ_d for different d is independent of each other, we parallelize the sampling procedure for different d, by OpenMP (`http://openmp.org/`). Since all sampling methods involve this and once for one β sample, it is still fair to compare the methods by the evolution along wall time, as long as the number of threads is the same.

Techniques to avoid overflow We need further special techniques to avoid the numerical overflow problem, which is caused by the modified Bessel function of the first kind $I_r(\cdot)$ in order r that is used in the normalization constant of vMF distribution (See Sec. 4 of the main paper). $I_r(\cdot)$ tends to be either zero or infinity on sides of some argument threshold when the order r is large. In our experiments $r = V/2 - 1$ is of order of thousands, and the behavior is obvious. To avoid trivial models, we have to choose hyper-parameters of SAM σ, κ_0 and κ_1 (acting as arguments of $I_r(\cdot)$) relatively large so that I_r is non-zero. But it then almost always overflows. Thanks to the fact that only its logarithm is required, we can try to directly calculate the logarithm. By noting that

$$\log I_r(x) = \log\left(\sum_{n=0}^{\infty} \frac{1}{n!\Gamma(n+r+1)}\left(\frac{x}{2}\right)^{2n+r}\right)$$

is the logarithm of a summation, we can use the log-sum trick: to calculate $\log(A + B)$ with only $a = \log A$ and $b = \log B$ (assume $a \geq b$) available, we can reformulate the target as

$$\log(A+B) = \log(\exp(a) + \exp(b)) = \log\big(\exp(a)\big(1 + \exp(b-a)\big)\big) = a + \log\big(1 + \exp(b-a)\big),$$

where $b - a \leq 0$ thus $1 + \exp(b - a) \leq 2$, so no numerical instability is met.

For specific implementation and parameters of our methods for the presented results, please refer to our codes.

References

[1] David M. Blei, Andrew Y. Ng, and Michael I. Jordan. Latent dirichlet allocation. *The Journal of Machine Learning Research*, 3:993–1022, 2003.

[2] Simon Byrne and Mark Girolami. Geodesic monte carlo on embedded manifolds. *Scandinavian Journal of Statistics*, 40(4):825–845, 2013.

[3] Changyou Chen, Nan Ding, and Lawrence Carin. On the convergence of stochastic gradient mcmc algorithms with high-order integrators. In *Advances in Neural Information Processing Systems*, pages 2269–2277, 2015.

[4] Tianqi Chen, Emily Fox, and Carlos Guestrin. Stochastic gradient hamiltonian monte carlo. In *Proceedings of the 31st International Conference on Machine Learning (ICML-14)*, pages 1683–1691, 2014.

[5] Herbert Goldstein. *Classical mechanics*. Pearson Education India, 1965.

[6] Matthew D. Hoffman and Andrew Gelman. The no-u-turn sampler: Adaptively setting path lengths in hamiltonian monte carlo. *Journal of Machine Learning Research*, 15(1):1593–1623, 2014.

[7] Sam Patterson and Yee Whye Teh. Stochastic gradient riemannian langevin dynamics on the probability simplex. In *Advances in Neural Information Processing Systems*, pages 3102–3110, 2013.

[8] Joseph Reisinger, Austin Waters, Bryan Silverthorn, and Raymond J. Mooney. Spherical topic models. In *Proceedings of the 27th International Conference on Machine Learning (ICML-10)*, pages 903–910, 2010.

[9] Aonan Zhang, Jun Zhu, and Bo Zhang. Sparse online topic models. In *Proceedings of the 22nd international conference on World Wide Web*, pages 1489–1500, 2013.